Aerodynamic performance evaluation of different cable-stayed bridges with composite decks

Rui Zhou[1], Yaojun Ge[2], Yongxin Yang[*2], Yanliang Du[1] and Lihai Zhang[3]

[1]*Institute of Urban Smart Transportation & Safety Maintenance, Shenzhen University, Shenzhen, 518060, China*
[2]*State Key Lab for Disaster Reduction in Civil Engineering, Tongji University, Shanghai 200092, China*
[3]*Department of Infrastructure Engineering, University of Melbourne, VIC 3010, Australia*

Abstract. The aerodynamic performance of long-span cable-stayed bridges is much dependent on its geometrical configuration and countermeasure strategies. In present study, the aerodynamic performance of three composite cable-stayed bridges with different tower configurations and passive aerodynamic countermeasure strategies is systematically investigated by conducting a series of wind tunnel tests in conjunction with theoretical analysis. The structural characteristics of three composite bridges were firstly introduced, and then their stationary aerodynamic performance and wind-vibration performance (i.e., flutter performance, VIV performance and buffeting responses) were analyzed, respectively. The results show that the bridge with three symmetric towers (i.e., Bridge I) has the lowest natural frequencies among the three bridges, while the bridge with two symmetric towers (i.e., Bridge II) has the highest natural frequencies. Furthermore, the Bridge II has better stationary aerodynamic performance compared to two other bridges due to its relatively large drag force and lift moment coefficients, and the improvement in stationary aerodynamic performance resulting from the application of different countermeasures is limited. In contrast, it demonstrates that the application of both downward vertical central stabilizers (UDVCS) and horizontal guide plates (HGP) could potentially significantly improve the flutter and vortex-induced vibration (VIV) performance of the bridge with two asymmetric towers (i.e., Bridge III), while the combination of vertical interquartile stabilizers (VIS) and airflow-depressing boards (ADB) has the capacity of improving the VIV performance of Bridge II.

Keywords: cable-stayed bridge; composite deck; tower system; wind tunnel tests; aerodynamic performance; passive aerodynamic countermeasures

1. Introduction

Cable-stayed bridges, have become increasing popular over the last fifty years because of their structural efficiency, economy and aesthetics, especial for medium and long-span of bridges (Daito *et al.* 2002). As a widely used deck configuration in long-span cable-stayed bridges around the world, a composite steel-concrete deck is composed of two structural edge girders, which is attached by transverse steel floor beams resulting in the advantages of small cross-section, light weight, low cost, and convenient construction (Collings 2013, Pedro *et al.* 2012). Typical examples include the two-tower Qingzhou Min River Bridge in Fuzhou (China) with a main span of 605m (Song *et al.* 2002), the three-tower cable-stayed Erqi Yangtze River Bridge in Wuhan (China) with two main spans of 616 m (Ge and Yang 2011), and the single-tower Manavgat Cable-Stayed Bridge (Turkey) with two main spans of 101 m (Atmaca *et al.* 2012, 2014). Furthermore, the design of multi-span and asymmetric composite cable-stayed bridges with composite girders are expected to be adopted for the bridges with a span ranging from 1000 m to 1200 m for the next coming years (Jorquera-Lucerga *et al.* 2016, Wang and Wu 2010, Chen *et al.* 2015, Fabbrocino *et al.* 2017). In practice, the design of long-span cable-stayed bridges is governed by the wind-induced dynamic responses. As the aerodynamic performance of the composite girder in form of a bluff body is obvious inferior to the streamlined box girder, one of the major problems in designing a cable-stayed bridge with composite girder is to overcome aerodynamic challenges due to the unfavourable shape of the deck, and therefore some aerodynamic amendments are required, such as fairings on both sides to give some streamlining, baffles between the main beams to divide the open void below the deck and limiting the torsional wind effects (Zhou *et al.* 2015). Major long-span cable-stayed bridges with composite girders around the world are listed in Table 1.

Aerodynamic performance evaluation of long-span cable-stayed bridges including stationary aerodynamic instability, flutter instability, vortex-induced vibration (VIV) and buffeting are usually conducted in wind tunnel tests (Scanlan and Jones 1990, Sakai *et al.* 1993 and Zhou *et al.* 2018). Stationary aerodynamic instability of bridges becomes significant when the deformed shape of the structure produces an increase in the value of the displacement-dependent wind loads imposed on the bridge structure. One of the major concern in bridge design is

---

*Corresponding author, Professor
E-mail: yang_y_x@tongji.edu.cn

Table 1 Typical examples of long-span cable-stayed bridges with composite girders

Bridge Name	Country	Main span (m)	Year Built	B/D	$\varepsilon = \frac{f_t}{f_b}$	Problems	Countermeasures
Alex-Fraser	Canada	465	1986	16	-	Flutter	Horizontal splitter
Co Chien	Vietnam	300	2011	6.87	2.28	VIV	Guide plates with 60°
2nd Ganjiang River	China	400	2014	9.73	2.01	VIV	Horizontal splitter+ vertical plates
Nanpu	China	423	1990	12.3	1.45	Flutter	vertical plates
Yangpu	China	602	1993	10.5	1.94	Flutter	vertical plates
Qinzhou Min River	China	605	1998	9.6	2.58	Flutter	Horizontal splitter+ vertical plates

flutter instability which causes dynamic instability, even structural catastrophe at a high wind velocity. In addition, VIV which exhibits limit cycle oscillations usually at low wind speed, affects the driving comfort and may reduce the service life of steel girders, and the buffeting response analysis becomes increasingly important with the increase of bridge span. Both buffeting displacement and internal forces responses gradually become larger with the increase of the wind speed, and could cause the fatigue damage and discomfort problems (Yeh *et al.* 2002, Koohi *et al.* 2014, Zhang *et al.* 2016). If the aerodynamic performance of a long-span cable-stayed bridge fails to meet the wind-resistance design requirement, it becomes necessary to improve the aerodynamic performance of bridges through application of effective aerodynamic countermeasures. Many types of passive aerodynamic countermeasures, such as stabilizers, flaps, fairings, spoilers, etc. have been implemented to improve the aerodynamic performance of bridges and the effectiveness of these countermeasures have also been experimentally investigated (Kubo *et al.* 2001, Fujino 2002, Zhou *et al.* 2019). For instance, to improve flutter performance, the overhanging deck and edge plates used in the Alex Fraser Bridge (Canada) (Irwin 1984), the apron boards and guide plates installed at the edge of the main girder in the Qingzhou Min River Bridge (China) (Song *et al.* 2002) and so on. Based on the results of wind tunnel tests, Murakamia (2002) compared the influence of central guard fences and rectangular members inside the main girders on flutter and VIV performance of a composite girder. Dong (2012) investigated the influence of inclined guide vanes on the flutter and VIV performance a cable-stayed bridge with a composite girder, while Zhou (2015) found that the combination of vertical stabilizers and airflow-depressing boards could effectively improve the aerodynamic performance of composite girder bridges. The focus of the above mentioned studies is mainly on the cable-stayed bridge with a composite girder and symmetrical same tower configurations. However, the influence of different tower types for cable-stayed bridges on aerodynamic performance are prominent (Shehata and Abdel 2014, Yang and Ge 2015), and the aerodynamic performance with different tower types and the effectiveness of countermeasures have not been fully understood so far. Therefore, it is important to further investigate the aerodynamic performance of composite

cable-stayed bridges with different tower types subjected to wind excitation.

The purpose of this study is to investigate the overall aerodynamic performance of three composite cable-stayed bridges with different tower configurations to identify the available aerodynamic countermeasure strategies. Firstly, the structural characteristics and Finite Element models of three typical cable-stayed bridges are presented and discussed. The stationary aerodynamic performance of these three bridges are then evaluated by conducting force-measured tests in wind tunnel and theoretical analysis. Finally, the flutter performance, VIV performance and buffeting responses of these bridges with countermeasures are quantified and compared through a series of wind tunnel tests and theoretical analysis, respectively. The present study has potential to result in guidelines for the design of long-span cable-stayed bridges with composite girders and the development of effective aerodynamic countermeasures.

2. Structural characteristics of three composite cable-stayed bridges

### 2.1 Structural characteristics of bridges

Three typical long-span cable-stayed bridges with composite girders of two I-shaped steel side beams and a concrete deck plate were selected in this study, in which two of these three bridges have two towers, and the other one has three towers. The structural layouts of these bridges and the cross-sections of composite girders are shown in Fig. 1, respectively. Bridge I (Fig. 1(a)) has the symmetrical structure with two main spans (616 m long each), three towers (209 m high each), and a composite main girder (32.3 m wide and 3.5 m deep). Bridge II (Fig. 1(b)) has a main span of 400 m, two inverted 124.5 m high Y-shaped pylons with 48 pairs of cables, and a composite main girder (29.2 m wide and 3.0 m deep). Bridge III (Fig. 1(c)) has asymmetrical structure with three spans (260 m, 388 m and 136 m long, respectively) and a composite girder (31.8 m wide and 3.25 m deep).

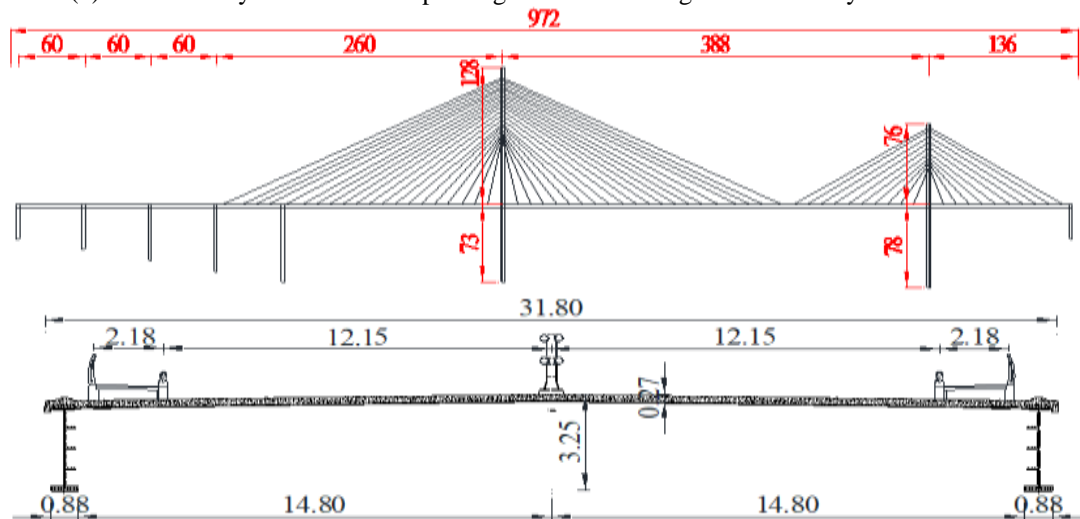### 2.2 Aerodynamic countermeasures

When the wind-resistance of bridges meet not the
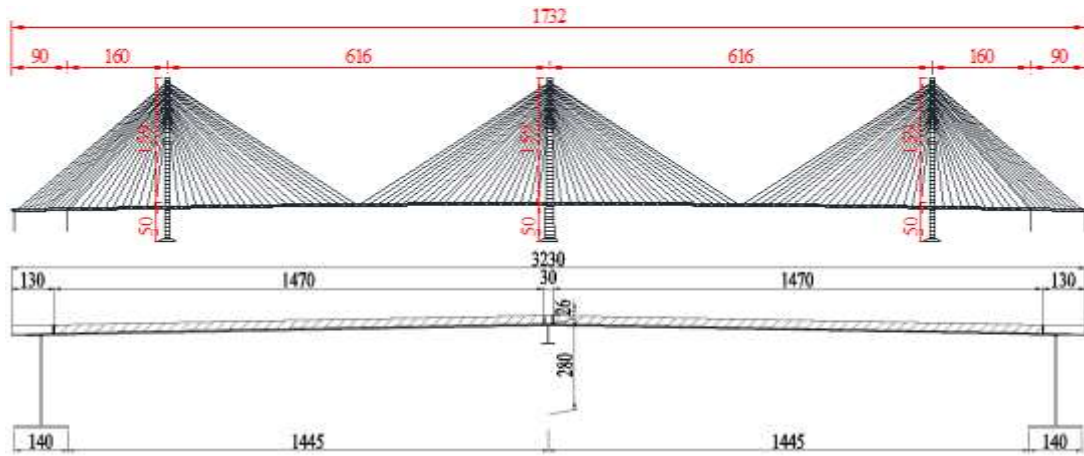
(a) Structural layout and the composite girder of the Bridge I with three symmetric towers
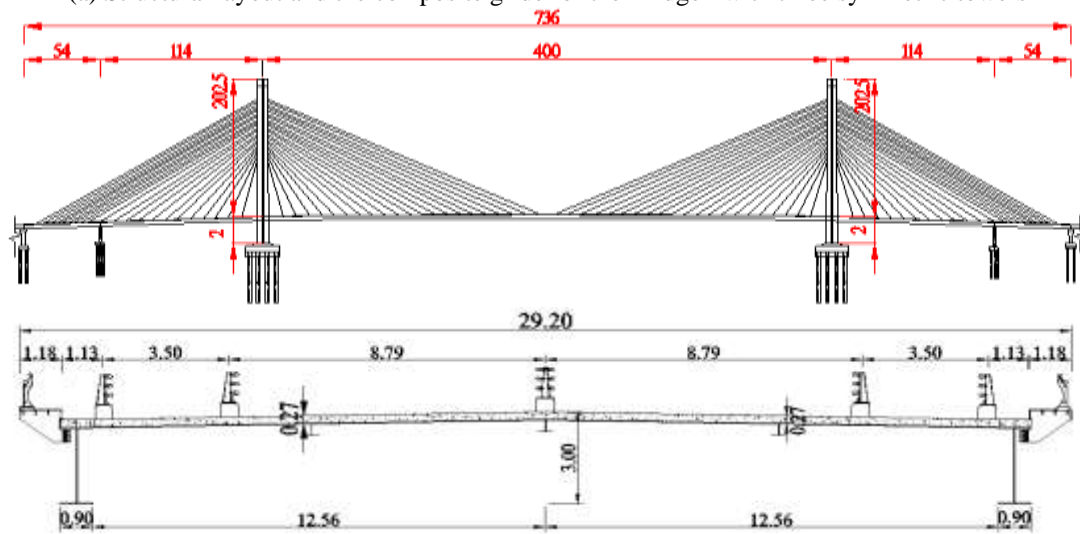
(b) Structural layout and the composite girder of the Bridge II with two symmetric towers

(c) Structural layout and the composite girder of the Bridge III with two asymmetric towers

Fig. 1 Structural layouts of the three cable-stayed bridges with composite girders (unit, m)

requirement of design, many types of passive aerodynamic countermeasures could be adopted, as shown in Fig. 2. Since the design of Bridge I with three towers leads to an excellent aerodynamic performance, aerodynamic countermeasures are not required to mitigate its wind-induced vibrations (Yang and Ge 2015). However, as the peak VIV responses of the Bridge II could be much larger than the allowable values of vertical VIV amplitude (i.e.,
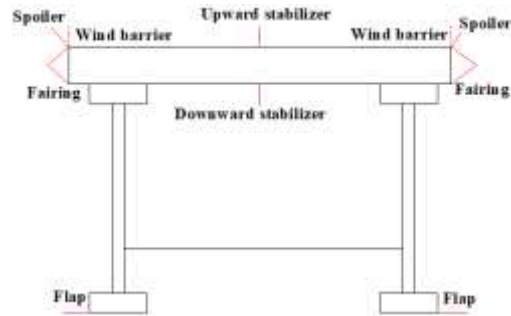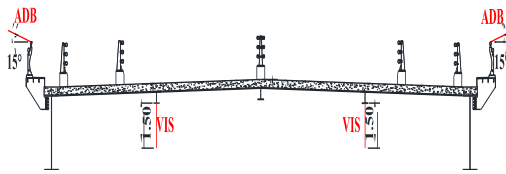
Fig.2 Examples of passive aerodynamic countermeasure
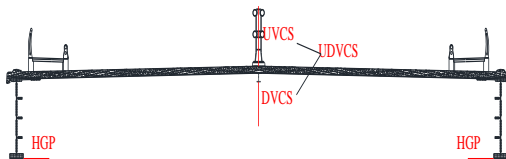

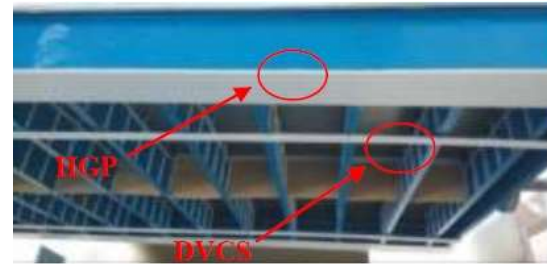(a) VIS+ADB of the Bridge II   (b) Sectional models of the Bridge II

Fig. 3 Schematic diagram of the Bridge II with two countermeasures

(a) UDVCS+HGP of the Bridge III   (b) Sectional models of the Bridge III

Fig. 4 Schematic diagram of the Bridge III with two countermeasures

0.111 m) and torsional VIV amplitude 0.216° (JTG/T D60-01-2004). A series of VIV tests about the combination of two aerodynamic countermeasures were conducted by varying the height of the vertical interquartile stabilizers (VIS) from 0.5 to 2.0 m and the angle of airflow-depressing boards (ADB) from 5° to 20°. The results show that the combination of a VIS height of 1.50 m and an ADB angle of 15° could effectively mitigate the risk of VIV responses. As for Bridge III, both the critical flutter wind velocity and peak VIV responses are much larger than the allowable values of vertical VIV amplitude (i.e., 0.143 m) and torsional VIV amplitude 0.289° (JTG/T D60-01-2004), the combination of two countermeasures (the upward and downward vertical central stabilizers (UDVCS) with the height of 2.78 m, and horizontal guide plates (HGP) with the height of 1.50 m) were used to simultaneously improve the flutter performance and mitigate the VIV responses. The schematic diagrams of the aerodynamic countermeasures for Bridge II and Bridge III with two towers are shown in Figs. 3 and 4, respectively.

2.3 Dynamic characteristics

Using commercial software package ANSYS, spatial three-dimensional (3D) finite element (FE) models of three cable-stayed bridges were established with consideration of structural nonlinearity, in which the main girder and main towers were modeled using 3D beam elements (BEAM4), while the main cables were modeled using 3D linear elastic truss elements (LINK10). Fig. 5 presents the triple-girder models of these bridges with composite girders (Zhu *et al*. 2000), in which the nonlinearity of the cables was taken into account using an equivalent tangent equation, the natural frequencies and mode shapes of these three bridges were calculated by using the subspace method (as shown in Table 2). It is found that the first natural frequencies of Bridge II are the largest among the three bridges, while the frequencies of Bridge I are lowest, regardless of the lateral, and vertical and torsional modes. Besides, the antisymmetrical modes are prior to the corresponding symmetrical modes for Bridge I with three towers, which is
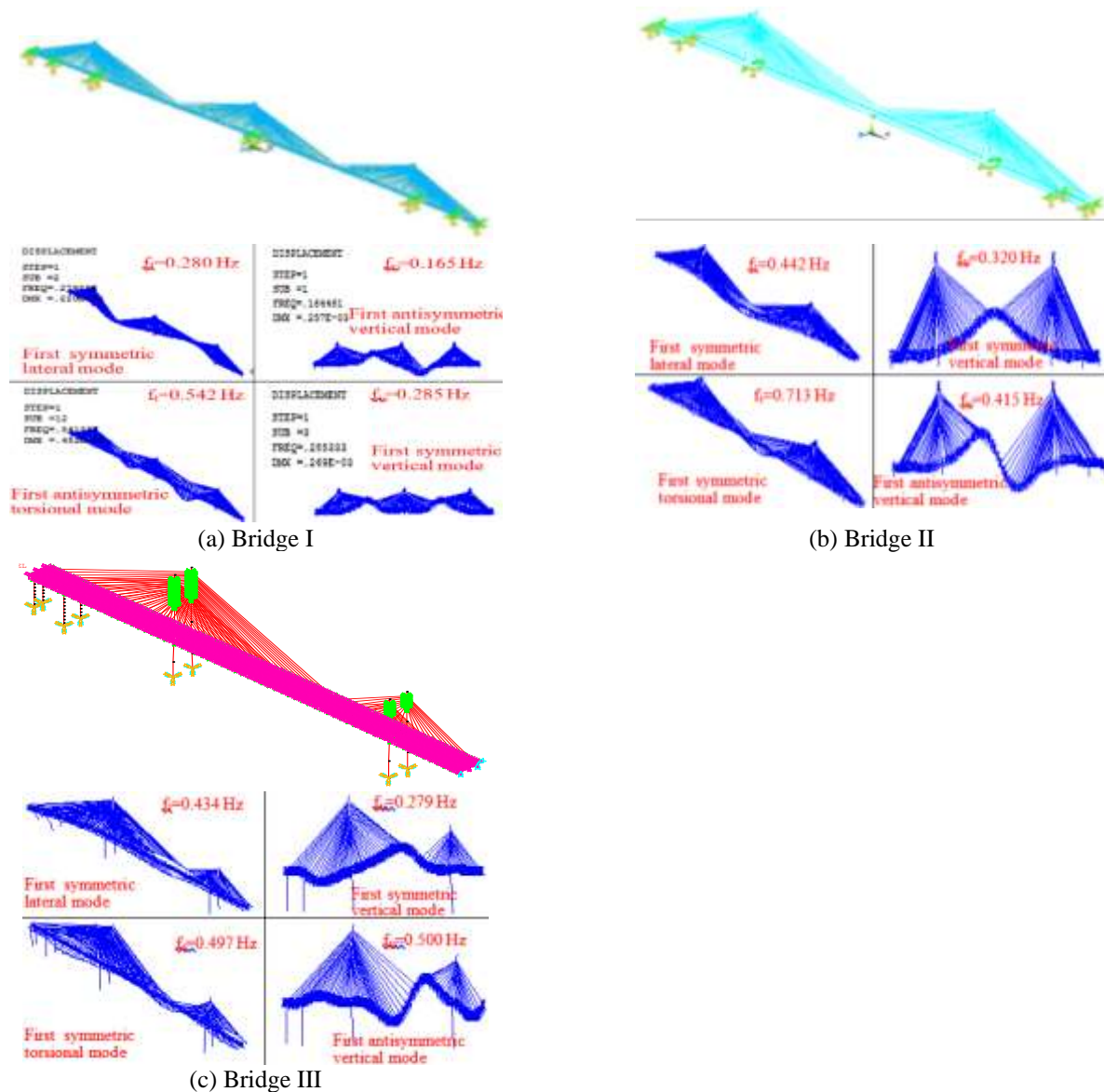
(a) Bridge I

(b) Bridge II

(c) Bridge III

Fig. 5 3D FE models and fundamental modal shapes of Bridge I, II & III

Table 2 Natural Mode Shapes and Frequencies of Bridge I, II & III

Mode shape	Frequency (Hz)		
	Bridge I	Bridge II	Bridge III
First symmetric vertical	0.285	0.320	0.279
First antisymmetric vertical	0.165	0.415	0.500
First symmetric lateral	0.311	0.442	0.434
First antisymmetric lateral	0.280	1.170	0.600
First symmetric torsional	0.549	0.713	0.497
First antisymmetric torsional	0.542	0.873	0.736

opposite to both the Bridge II and Bridge III with two towers.

3. Stationary aerodynamic performance of three cable-stayed bridges

3.1 force-measured tests
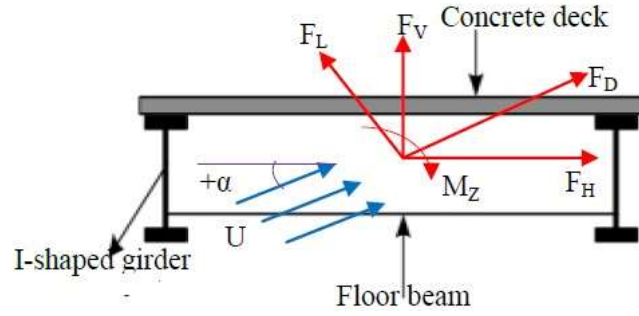
Fig. 6 Three components of static aerodynamic forces (F_D, F_L and M_Z)
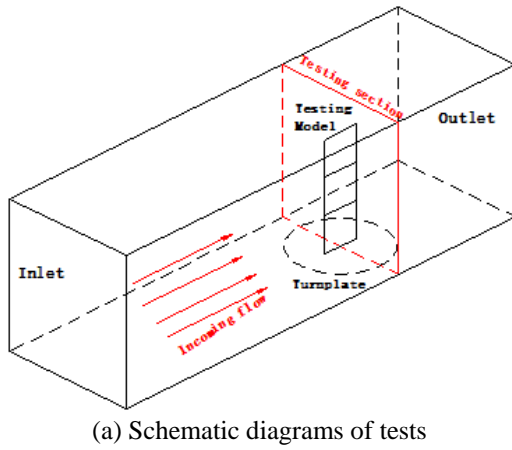
(a) Schematic diagrams of tests   (b) Sectional models

Fig. 7 Force-measured tests of Bridge I, II & III

Aerodynamic force coefficients play an important role in controlling the stationary aerodynamic performance of bridges. Three components of aerodynamic forces per unit length acting on the composite girder are the drag force (F_D), lift force (F_L) and pitching moment (M_z) (Fig. 6), given by

$$C_D=\frac{F_D}{\frac{1}{2}\rho U^2 H}, C_L=\frac{F_L}{\frac{1}{2}\rho U^2 B}, C_M=\frac{M_Z}{\frac{1}{2}\rho U^2 B^2} \qquad (1)$$

$$F_D=F_H cos\alpha+F_V sin\alpha, \ F_L=-F_H sin\alpha+F_V cos\alpha \qquad (2)$$

where C_D, C_L and C_M are coefficients of drag force, lift force, and pitching moment in the wind axes, respectively; F_H, F_V and M_T are the drag force, lift force and pitching moment in the body axes, respectively; ρ is the air density; U is the wind velocity; and $+\alpha$ is the positive effective wind attack angle. B and H is the width and height of the composite girder, respectively.

As shown in Fig. 7, the sectional models of three composite girders with the same geometrical scale ratio of 1:60 were tested in the TJ-2 Boundary Layer Wind Tunnel at Tongji University, respectively. A wind velocity of 10 m/s was used throughout the force-measured tests with 25 wind attack angles ranging from -12° to +12° with an increment of 1°. Three static aerodynamic coefficients including the C_D, C_L and C_M of three bridges are compared and then these coefficients for two bridges (e.g., Bridge II and III) with or without aerodynamic countermeasures are also described.

It can be seen that the values of both C_D and C_M for Bridge II are the largest among the three bridges under the negative angles, whereas the values of C_D and C_L for Bridge I are the largest with the wind angle is greater than 9 degree. In total, the values of C_D, C_L and C_M for Bridge III are the smallest among the three bridges in Fig. 8. On the other hand, the values of C_D and C_L for Bridge II after installing VIS and ADB under the positive angles are significantly larger than those without countermeasures, while the values of C_D and C_L for Bridge III after installing UDVCS and HGP under the negative angles are obviously larger than those without countermeasures. In addition, the values of C_M for Bridge II and III with countermeasures are smaller than those without countermeasures.

3.2 Stationary aerodynamic performance

A numerical calculation based on the optimum iteration method (Zhang *et al.* 2013) is used to investigate the stationary aerodynamic performance of three cable-stayed bridges with consideration of the aerodynamic force nonlinearity and the geometric nonlinearity. In this study, the torsional divergence critical wind velocities (U_{td}) of Bridge II and III with countermeasures under three wind attack angles are determined based on the above results of stationary aerodynamic forces. As shown in Table 3, the values of U_{td} of three bridges are much larger than the corresponding allowable wind velocities U_{ab} (JTG/T D60-01-2004) under three wind attack angles, and therefore

(a) C_D of the three bridges

(b) C_L of the three bridges

(c) C_M of the three bridges

(d) Static aerodynamic coefficients of Bridge I

(e) Coefficients of Bridge II
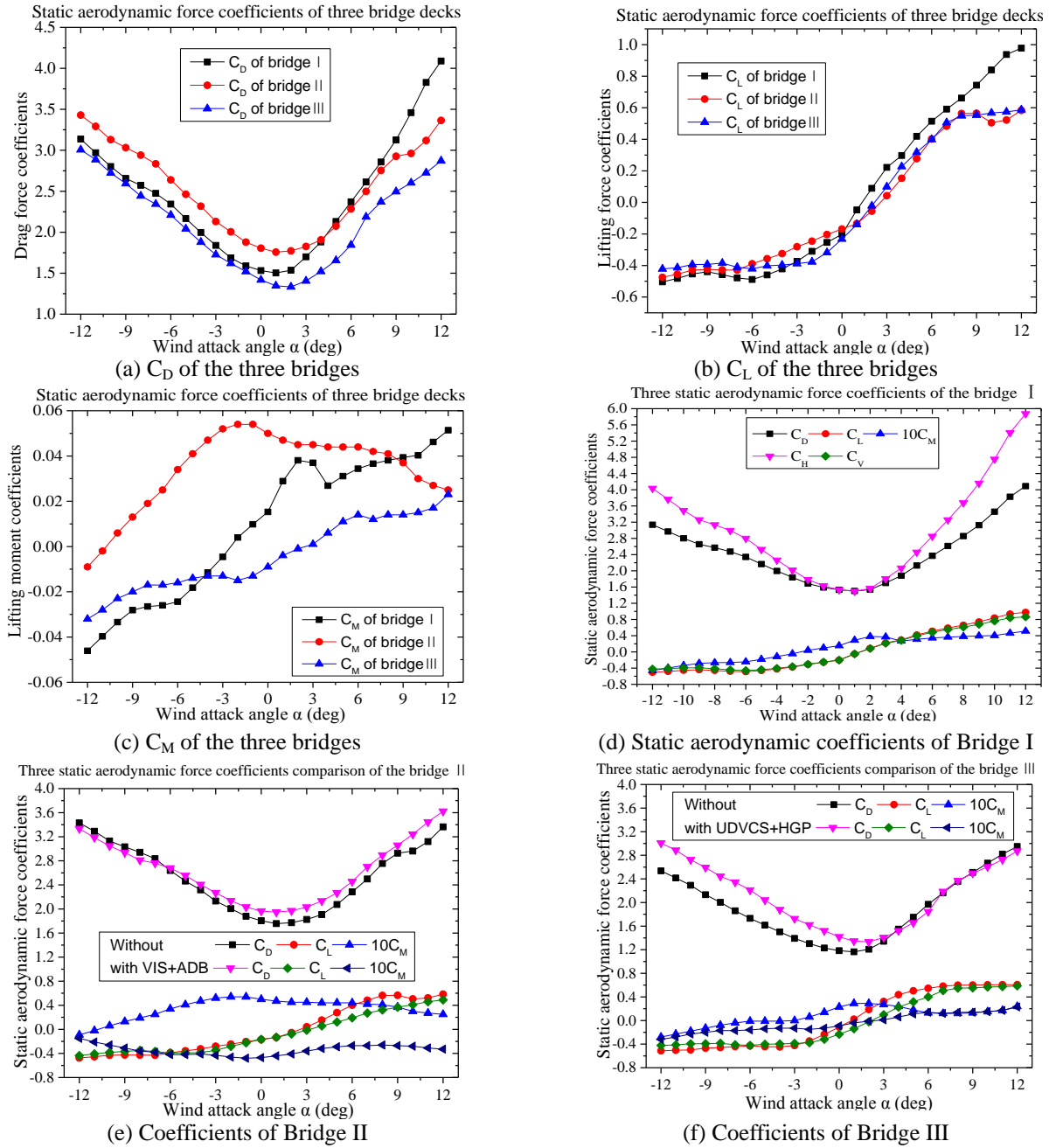

(f) Coefficients of Bridge III

Fig. 8 Comparison of the static aerodynamic coefficients of Bridge I, II & III

fulfil the requirement of stationary aerodynamic performance. Furthermore, the U_{td} of Bridge I with three towers (>100 m/s) are much smaller than both the Bridge II (>260 m/s) and Bridge III (220 m/s) with two towers. Most importantly, the U_{td} of Bridge III increases from 220 m/s to 250 m/s after the installation of countermeasures. In summary, the stationary aerodynamic performance of Bridge II is the best among the three bridges, while the performance of Bridge I is the worst. The implementation of the countermeasures can slightly improve the stationary aerodynamic performance of Bridge II and III.

To further explore the stationary aerodynamic performance, the structural displacements (e.g., vertical, horizontal and torsional displacement) at midpoint (1/2L) of bridge decks of three bridges (and Bridge II & III with countermeasures) were determined under an unfavourable wind attack angle (i.e., +3°). As described in Fig. 9, the absolute values of vertical, horizontal and torsional displacements of the three bridges gradually increase with the increase of wind velocity, and the growth rates of all the three displacements of Bridge I are the fastest among the three bridges. Specifically, there is a rapid increase in the torsional displacement of the Bridge I before the $U_{td} = 100$ m/s, and all the three displacements of the Bridge III change
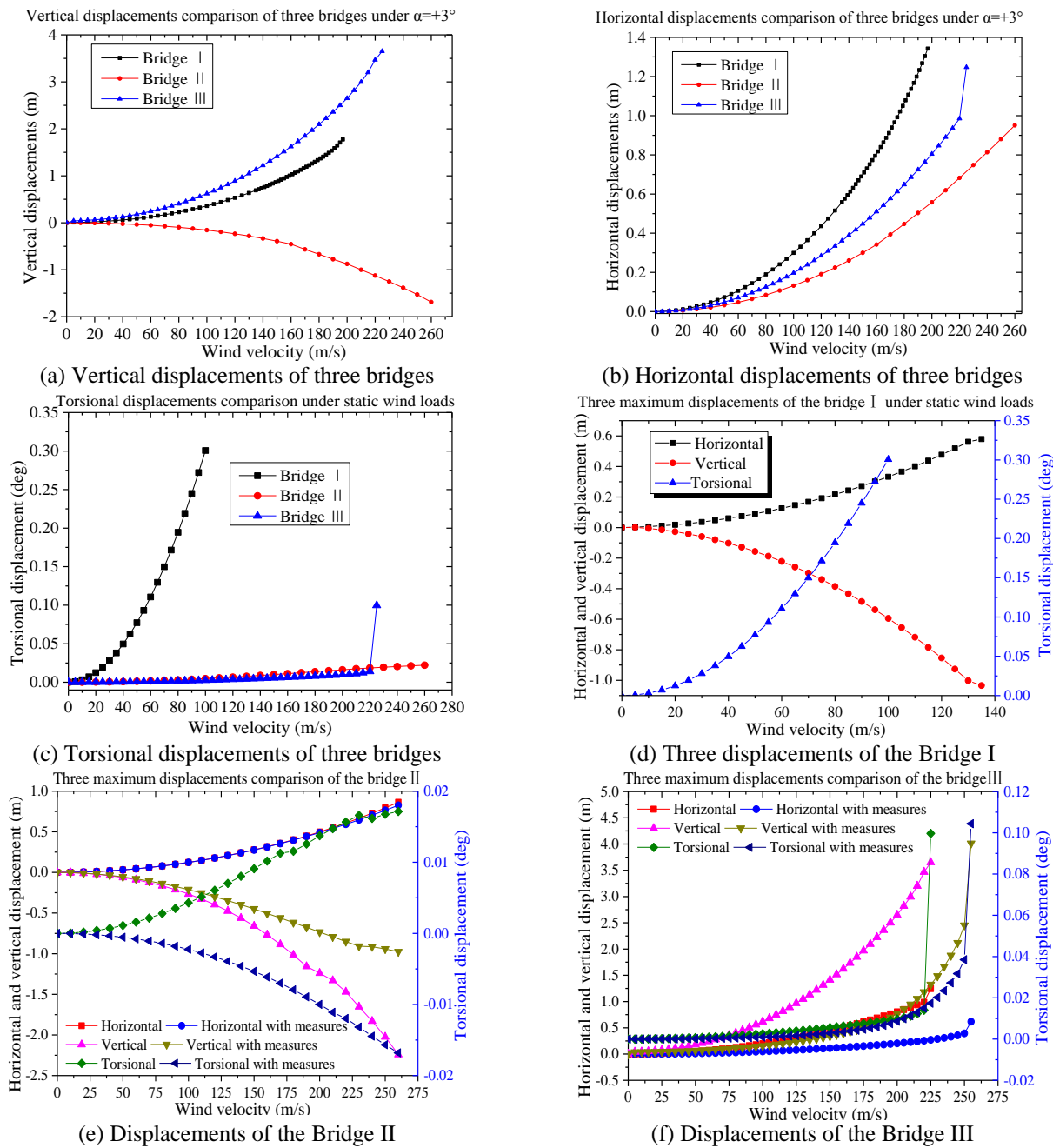
(a) Vertical displacements of three bridges

(b) Horizontal displacements of three bridges

(c) Torsional displacements of three bridges

(d) Three displacements of the Bridge I

(e) Displacements of the Bridge II

(f) Displacements of the Bridge III

Fig. 9 Displacement responses of Bridge I, II & III

Table 3 Torsional divergence critical wind velocities (U_{td}) for the bridges

α	Three original bridges with different structural systems			Two bridges with countermeasures	
	Bridge I	Bridge II	Bridge III	Bridge II with VIS+ADB	Bridge III with UDVCS+HGP
-3°	>100	>260	>250	>260	>250
0°	>100	>260	>250	>260	>250
+3°	>100	>260	220	>260	250
U_{ab}	43.9	37.9	76.1	37.9	76.1

abruptly at the U_{td} =250 m/s. In addition, it is observed that the vertical displacement of Bridge II is always negative with a relatively small growth rate. On the other hand, the implementation of countermeasures has slight impact on the horizontal displacement of Bridge II, whereas the vertical displacement of Bridge II become smaller after the installation of countermeasures. It is interesting that the torsional displacements of Bridge II with countermeasures are always negative, which is contrary to those without countermeasures. The three displacements of the Bridge III become significantly smaller after the installation of countermeasures, especially for the vertical displacement.

(a) Experiment set-up

(b) Sectional models

Fig. 10 Schematic diagrams of flutter tests for Bridge I, II & III

Table 4 Structural properties of the prototype and sectional models for Bridge I, II & III

Properties	Bridge I		Bridge II		Bridge III	
	Prototype	Sectional model	Prototype	Sectional model	Prototype	Sectional model
Width (B)/m	32.3	0.538	29.2	0.487	31.8	0.530
Depth (D) /m	3.5	0.058	3.0	0.050	3.25	0.054
Length (D) /m	104	1.740	104	1.740	104	1.740
Mass (M)/ kg/m	47227	13.12	38801	10.778	49768	13.824
Inertia I_M/ kg·m²/m	4572630	0.353	2864466	0.221	4444740	0.343
Vertical frequency (f_v)/ Hz	0.165	1.65	0.358	4.081	0.279	3.348
Torsional frequency (f_t) / Hz	0.542	5.42	0.722	8.228	0.497	5.952
Wind velocity ratio	1	6	1	5.26	1	5
Vertical damping (ξ_v)	0.7	0.7	0.97	0.97	1.02	1.02
Torsional damping (ξ_t)	0.6	0.6	0.73	0.73	0.93	0.93

4. Wind-induced vibrations of three cable-stayed bridges

4.1 Flutter performance

As shown in Fig. 10, the flutter tests on two-dimensional rigid sectional models of the three composite girders were conducted in a 3 m (width)×2.5 m (height) test section of the TJ-2 wind tunnel in Tongji University, China. All the geometric scales of the three sectional models are 1:60, and the major structural parameters including geometric dimensions, mass characteristics, fundamental frequencies and structural damping of the prototype bridge and their scaled sectional models are listed in Table 4. It should be mentioned that the aerodynamic countermeasures on these bridges were adopted to make the structural

dynamic characteristics consistent in all testing cases.

The purpose of the flutter tests was to investigate the influence of different tower systems on the critical flutter wind velocity (U_{cr}) of cable-stayed bridges, and the U_{cr} of the three bridges under three wind attack angles (i.e., +3°, 0° and -3°) are presented in Table 5. Regardless of wind attack angle, the U_{cr} of Bridge II is the largest among the three bridges, and the U_{cr} of Bridge III smallest. The U_{cr} of both Bridge I and Bridge II are larger than their corresponding allowable wind velocity, whereas the U_{cr} of Bridge III under the angle of +3° (i.e., 50 m/s) is smaller than the allowable wind velocity (i.e., 59 m/s). This indicates that it is necessary to improve the flutter performance of the Bridge III by implementing aerodynamic countermeasures. Besides, it shows that a

Table 5 Critical flutter wind velocities (U_{cr}) of Bridge I, II & III

α	Three bridges without countermeasures			Two bridges with countermeasures	
	Bridge I	Bridge II	Bridge III	Bridge II with VIS+ADB	Bridge III with UDVCS+HGP
-3°	86.5	100.5	73.5	114.0	75.0
0°	74.0	90.2	55.0	93.0	67.5
+3°	59.8	70.0	50.0	78.0	73.0
U_{ab}	53.7	47.0	59.0	47.0	59.0
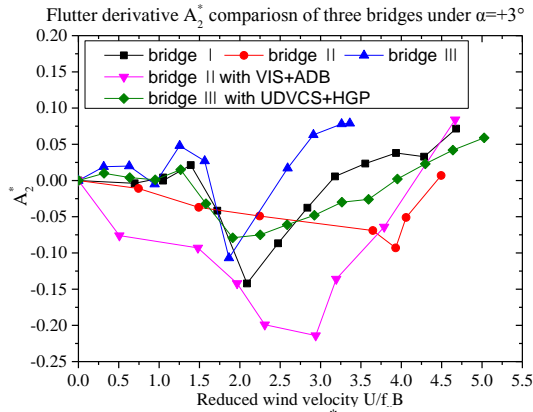
(a) Flutter derivatives A_2^* comparison
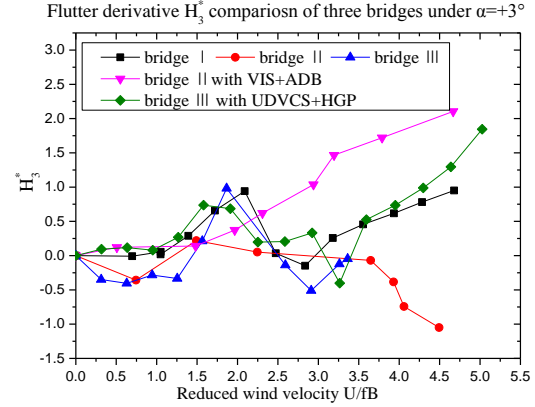
(b) Flutter derivatives H_3^* comparison
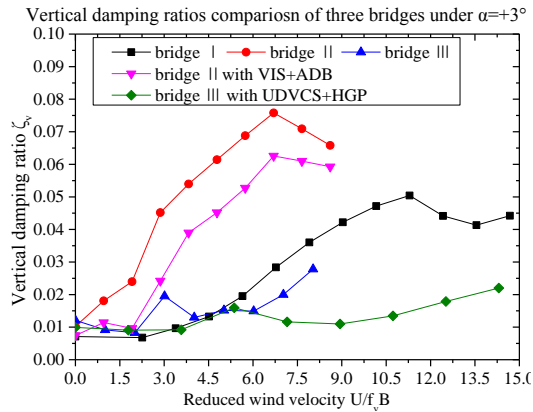
(c) Vertical damping ratios comparison
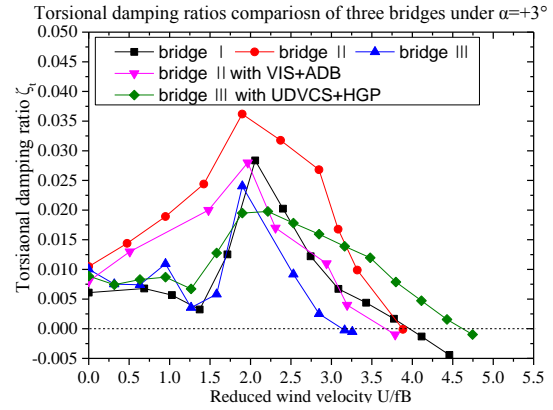
(d) Torsional damping ratios comparison

Fig. 11 Flutter derivatives, damping ratios for Bridge I, II & III

wind attack angle of +3° results in the smallest U_{cr}, and therefore is the most unfavorable wind attack angle for cable-stayed bridges with composite girders. In additional, the installation of VIS and ADB can significantly increase the U_{cr} of Bridge II (e.g., the U_{cr} of Bridge II under the wind attack angle of +3° can increase from 70 m/s to 78 m/s). The results indicate that the combination of VIS and ADB could significantly enhance aerodynamic performance of Bridge II with two asymmetrical towers. Further, it is noted that the use of UDVCS and HGP could increase the U_{cr} of Bridge III from 50 m/s to 73 m/s with a growth rate of 46%, and therefore enhances the flutter performance of the bridge with two asymmetrical towers.

The flutter derivatives and total structural damping of the three bridges with countermeasures were identified by using the improved least squares method (Scalan and Tomko 1971), and two crucial flutter derivatives (i.e., A_2^* and H_3^*) under the unfavorable angle of +3° are presented in Fig. 11. The value of A_2^* firstly decreases and then generally increases with the increase of wind speed, where the reduced wind velocity corresponding to the smallest A_2^* are about 3.0 and 4.0 for the Bridge II without and with countermeasures, respectively. The value of H_3^* gradually increases with the increase of wind speed, and the installation of countermeasures results in a higher value of H_3^*. Furthermore, the vertical damping ratio ξ_v presents an upward with the increase of wind speed, and the value of

Table 6 Critical flutter wind velocities (U_{cr}) for Bridge I, II & III

	Three bridge structural systems		
	Bridge I	Bridge II	Bridge III
Torsional-vertical frequency ratio	3.285	2.017	1.778
Vad der Put	50.2	31.0	29.7
Selberg	55.1	38.4	35.9
Tongji University	53.5	30.9	30.2
Experimental results	59.8	70.0	50.0
U_{ab}	53.7	47.0	59.0

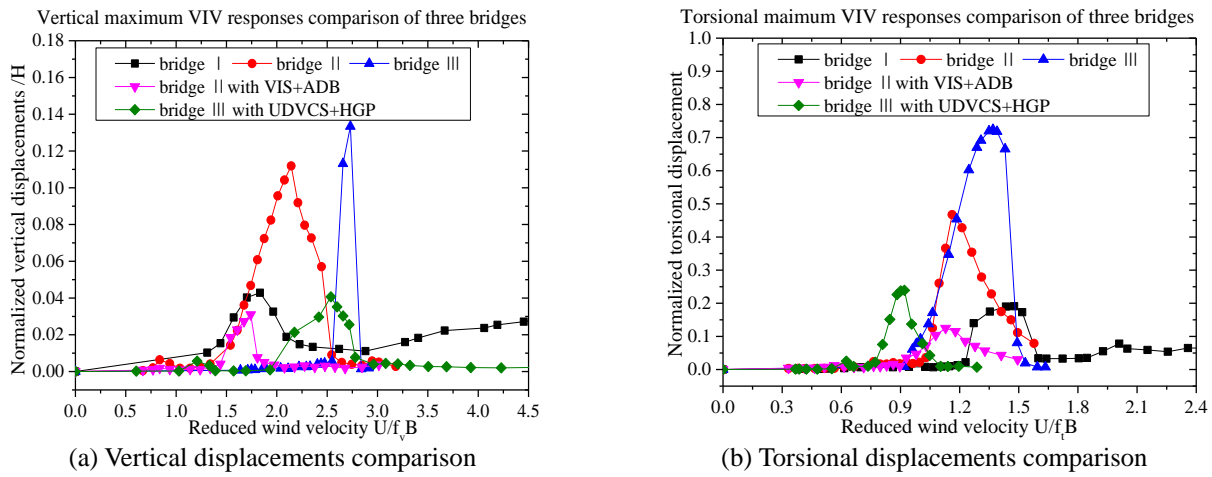(a) Vertical displacements comparison   (b) Torsional displacements comparison

Fig. 12 VIV responses comparison of Bridge I, II & III

ξ_v significantly become smaller after the installation of countermeasures. Moreover, the torsional damping ratio ξ_t initially increases with the increase of wind speed, reach to its peak value at the reduced wind velocity of about 2.0, and then shifts from the positive to negative territory on the flutter onset. The reduced wind velocities are the critical flutter wind velocities when the values of ξ_t are zero, and the ξ_t of Bridge III without and with countermeasures are the smallest and largest among these cases, respectively. Thus, the torsional damping ratio is the most important aerodynamic damping component of heaving-torsional coupled flutter.

In addition, the critical flutter wind velocities of the three cable-stayed bridges having different torsional-vertical frequency ratios can be predicted using the empirical formulas with two dimensional flutter analysis, such as Vader Put function (Van der Put 1976), Selberg equation (Selberg 1963) and Tongji University ($U_{cr}=2.5\times\sqrt{\mu\times\frac{r}{b}}\times B\times f_t$) (JTG/T D60-01-2004). The prediction results are shown in Table 5. It can be seen that the predict values of U_{cr} for these bridges are much smaller than the allowable wind velocities. The U_{cr} of these bridges increases with the increase of the torsional-vertical frequency ratio, and U_{cr} of Bridge I is the largest among the three bridges. By comparing the predicted results with the

experimental measurements (Table 6), it shows that the empirical formulas with two dimensional flutter analysis of bridges could not accurately predict the U_{cr} of these three bridges

4.2 VIV performance

The VIV tests involving three sectional models of these three bridges were also conducted in the TJ-2 Boundary Layer Wind Tunnel at Tongji University. The geometric scale ratios used in VIV tests are the same as that used in flutter tests. According to the JTG/T D60-01-2004, the allowable amplitude limitation of the heaving with $0.04/f_h$ and torsional VIV of these prototype bridges with $4.56/(Bf_t)$ are defined. Table 7 shows the detailed VIV responses (*i.e.* Lock-in wind velocity, the maximum amplitudes, allowable amplitudes and control effects of the measures) in vertical and torsional DOF of three bridges without and with counter measures under three wind attack angles of -3°, 0° and +3°. The maximum VIV responses normalized to the height of composite girder are described in Fig. 12.

Table 6 also shows that both the maximum vertical and torsional VIV responses of Bridge I are smaller than the allowable amplitudes, and thus the VIV performance of Bridge I meet the design requirements. After installing

Table 7 VIV responses of Bridge I, II & III

Types of bridges	Direction	α	Lock-in wind velocity (m/s)	Maximum amplitude	Allowable amplitudes [26]	Control effects
Bridge I	Vertical	-3°	7.7~12.6	0.159 m	0.243m	No
		0°	7.0~9.1	0.110 m		No
		+3°	7.0~9.1	0.114 m		No
	Torsional	-3°	20.8~28.0	0.207°	0.261°	No
		0°	12.9~24.4	0.198°		No
		+3°	16.5~24.4	0.133°		No
Bridge II	Vertical	-3°	14.00~20.30	0.058 m	0.111m	No
		0°	15.05~21.35	0.088 m		No
		+3°	17.50~26.60	**0.335 m**		**Yes**
	Torsional	-3°	21.35~31.50	0.073°	0.216°	No
		0°	23.45~27.30	0.147°		No
		+3°	22.40~31.50	**0.468°**		**Yes**
Bridge III	Vertical	-3°	11.63~17.42	**0.221 m**	0.143m	**Yes**
		0°	12.92~19.06	**0.306 m**		**Yes**
		+3°	22.61~25.19	**0.434 m**		**Yes**
	Torsional	-3°	15.83~24.41	0.237°	0.289°	No
		0°	19.06~22.61	0.154°		No
		+3°	14.54~22.61	**0.724°**		**Yes**
Bridge II with VIS and ADB	Vertical	-3°	15.05~20.65	0.093 m	0.143m	-60.3%
		0°	14.00~17.50	0.072 m		18.2%
		+3°	14.00~17.15	0.042 m		87.5%
	Torsional	-3°	22.75~31.50	0.125°	0.289°	-71.2%
		0°	18.55~31.50	0.094°		36.1%
		+3°	22.40~31.50	0.075°		84.0%
Bridge III with UDVCS and HGP	Vertical	-3°	10.14~14.90	0.132 m	0.143m	40.3%
		0°	6.34~7.24	0.022 m		92.8%
		+3°	6.34~8.88	0.017 m		96.1%
	Torsional	-3°	13.31~22.19	0.219°	0.289°	7.6%
		0°	12.68~18.07	0.239°		-55.2%
		+3°	13.95~16.80	0.041°		94.3%

countermeasures, the maximum vertical VIV response of Bridge II decreases from 0.335 m to 0.093 m, while the maximum torsional VIV response of Bridge II decreases from 0.468° to 0.125°. In addition, the results show that the combination of VIS and ADB can effectively bring the VIV response of Bridge II below the allowable amplitude. For Bridge III, under the unfavorable wind attack angle of +3°, the installation of countermeasures can decrease the maximum vertical VIV response from 0.434 m to 0.132 m, and the torsional VIV response from 0.724° to 0.239°. Further, it demonstrates that the countermeasures can effectively reduce vertical amplitude of Bridge II and torsional amplitude of Bridge III.

4.3 Buffeting responses

Based on the quasi-steady assumption (Scalan and Tomko 1971), the turbulence energy distribution of the wind with respect to frequency can be formulated using the power spectrums. Thus, the frequency domain buffeting analysis can use the Kaimal spectrum and Panofsky spectrum described in Eq. (3) as the input horizontal and vertical spectrum, respectively

$$\frac{nS_u(n)}{u_*^2} = \frac{200f}{(1+50f)^{5/3}}, \frac{nS_w(n)}{u_*^2} = \frac{6f}{(1+4f)^2} \tag{3}$$

Table 8 Maximum buffeting displacements at the 1/2L of Bridge I, II & III

Bridges	aerodynamic admittance	Horizontal displacement(m)	Vertical displacement(m)	Lateral displacement(m)	Around horizontal angle (°)	Around vertical angle (°)	Around lateral angle (°)
Bridge I	1	0.006	1.303	0.11	0.32661	0.02865	0.34953
	Sears function	0.003	0.774	0.072	0.12606	0.01719	0.17763
Bridge II	1	0.0007	0.2316	0.0356	0.083658	0.000997	0.021717
	Sears function	0.0003	0.0840	0.0216	0.021545	0.000131	0.008939
Bridge III	1	0.0091	0.4351	0.3532	0.21774	0.13752	0.2292
	Sears function	0.0064	0.2936	0.1607	0.09741	0.06303	0.14325
Bridge II with VIS and ADB	1	0.0005	0.1930	0.0942	0.111162	0.002149	0.018221
	Sears function	0.0028	0.0688	0.0571	0.028478	0.000348	0.007506
Bridge III with UDVCS and HGP	1	0.1090	0.3970	0.0348	0.570135	0.027676	0.373596
	Sears function	0.0906	0.2200	0.0219	0.233211	0.01146	0.245244

Table 9 Maximum buffeting internal forces at the 1/2L of Bridge I, II & III

Bridges	aerodynamic admittance	Axial force (N)	Vertical shear force (N)	Horizontal shear force(N)	Torsional moment (N. m)	Horizontal bending moment (N. m)	Vertical bending moment (N. m)
Bridge I	1	8.90E+06	1.05E+06	4.74E+05	2.49E+05	1.74E+07	7.81E+07
	Sears function	4.49E+06	6.81E+05	1.59E+05	7.95E+04	6.60E+06	5.19E+07
Bridge II	1	8.59E+06	3.63E+05	3.41E+05	8.06E+06	7.99E+07	1.50E+07
	Sears function	8.49E+06	1.77E+05	1.03E+05	1.93E+06	7.63E+07	7.38E+06
Bridge III	1	1.29E+07	8.21E+05	6.04E+06	2.48E+07	8.95E+08	1.57E+07
	Sears function	1.01E+07	5.49E+05	2.75E+06	1.13E+07	4.08E+08	1.02E+07
Bridge II with VIS and ADB	1	8.64E+06	3.15E+05	7.52E+05	4.99E+06	2.11E+08	1.26E+07
	Sears function	7.73E+06	1.46E+05	5.12E+05	2.66E+06	1.97E+08	6.14E+06
Bridge III with UDVCS and HGP	1	1.63E+07	3.51E+05	3.12E+06	2.10E+07	1. 62E+08	9.25E+07
	Sears function	1.11E+07	1.65E+05	1.74E+06	1.45E+07	1. 00 E+08	8.98E+07

The relationship among three turbulence intensities at the surface height of the composite girders are assumed to be $I_u:I_v:I_w = 1:0.88:0.5$, where the I_u, I_v and I_w is the perpendicular to bridge span, along-bridge span and vertical turbulence intensity, respectively. In order to compare the three-dimensional buffeting responses of the three bridges, the aerodynamic admittances of buffeting forces on composite girders are modelled by Sears' function of potential flow theory (Sears 1941) and 1 as the lower and upper limit (neglect the unsteady characteristic and the span-wise correlation of the bridge deck). The maximum buffeting displacement responses and internal forces in six directions at the midpoint (1/2L) of the three bridges under the wind attack angle of 0° are shown in Tables 8 and 9, respectively. All the wind speed of buffeting responses are 32 m/s according to the design reference wind speed (JTG/T D60-01-2004). Table 8 shows that the vertical displacement (0.774 m~1.303 m) and torsional displacement (0.126°~0.327°) of Bridge I and the lateral displacement of Bridge III (0.16 m~0.35 m) are the largest among the three bridges, respectively. In addition, for Bridge II, the installation of the countermeasures can reduce the buffeting vertical displacement of the bridge but increase other displacements to some extent. For Bridge III, the implementation of countermeasures can decrease the lateral displacement of the bridge but increase the torsional displacements. The results from Table 8 show that the axial force and torsional moment of Bridge II are the largest among the three bridges, and the installation of countermeasures has slight impact on the internal forces of the bridges. In summary, the countermeasures cannot significantly improve the buffeting responses of Bridge II and III.

5. Conclusions

In this study, a series of wind tunnel tests in conjunction with theoretical analysis were conducted to investigate the overall aerodynamic performance of three composite cable-stayed bridges with different tower configurations and

effectiveness of different countermeasures. The followings are the major conclusions

• The Bridge I with three symmetric towers has the smallest natural frequencies among the three bridges since its anti-symmetrical modes are prior to the corresponding symmetrical modes. The natural frequencies of the Bridge II with two symmetric towers are larger than that of the Bridge III with two asymmetric towers.

• The Bridge II has the highest torsional divergence critical wind velocities among the three bridges due to its relatively large C_D and C_M . The aerodynamic countermeasures has the capability of increasing the values of U_{td} of both Bridge II and III through the increasing the three aerodynamic force coefficients of the two bridges.

• The application of both VIS+ADB could improve the VIV performance of Bridge II, while the combination of UDVCS+HGP can significantly improve the flutter and VIV performance of Bridge III. Although the Bridge I has a relatively better overall wind-resistance performance, more attention should be paid to its buffeting displacement responses.

This study mainly focuses on investigating the effects of tower configuration of the cable-stayed bridges on the aerodynamic performance of the bridges. However, the configuration of other structural systems (i.e., cable), which also play an important role in controlling the aerodynamic performance of the bridges, should be further understood. Besides, further research work is still required to understand the influence of other passive countermeasures on the aerodynamic performance of long-span cable-stayed bridges.

Acknowledgments

References

Atmaca, B. and Ate, S. (2012), "Construction stage analysis of three-dimensional cable-stayed bridges", *Steel Compos. Struct.*, **12**(5), 413-426. https://doi.org/10.12989/scs.2012.12.5.413.

Atmaca, AB., Yurdakul, M. and Ates, S. (2014), "Nonlinear dynamic analysis of base isolated cable-stayed bridge under earthquake excitations", *Soil Dyn. Earth. Eng.*, **66**, 314-318. https://doi.org/10.1016/j.soildyn.2014.07.013.

Cheng, B., Wu, J. and Wang, J.L. (2015), "Strengthening of perforated walls in cable-stayed bridge pylons with double cable planes", *Steel Compos. Struct.*, **18**(4), 811-831. https://doi.org/10.12989/scs.2015.18.4.811.

Collings, D. (2013), Steel-concrete composite bridges: Designing with Eurocodes, 2nd Edition. Thomas Telford Ltd, London, UK. ICE Publishing.

Daito, Y., Matsumoto, M. and Araki, K. (2002), "Torsional flutter mechanism of two-edge girders for long-span cable-stayed bridge", *J. Wind Eng. Ind. Aerod.*, **90**(12-15), 2127-2141. https://doi.org/10.1016/S0167-6105(02)00329-X.

Dong, R., Yang, Y.X. and Ge, Y.J. (2012), "Wind tunnel test for aerodynamic selection of Π shaped deck of cable-stayed bridge", *J. Harbin Inst. Tech.*, **44**(10), 109-114. (In Chinese)

Fabbrocino, F., *et al.* (2017), "Optimal prestress design of composite cable-stayed bridges", *Compos Struct.*, **169**(1), 167-172. https://doi.org/10.1016/j.compstruct.2016.09.008.

Fujino, Y. (2002), "Vibration, control and monitoring of long-span bridges-recent research, developments and practice in Japan", *J. Constr. Steel Res.*, **58** (1),71-97. https://doi.org/10.1016/S0143-974X(01)00049-9.

Ge, Y.J. and Yang, Y.X. (2011), "Wind-resistant performance investigation for Wuhan Erqi Yangtze River Bridge. Technical Report WT201044", State Key Laboratory for Disaster Reduction in Civil Engineering, Shanghai. (In Chinese)

Koohi, R., Shahverdi, H. and Haddadpour. H. (2014), "Nonlinear aeroelastic analysis of a composite wing by finite element method", *Compos. Struct.*, **113**:118-126. https://doi.org/10.1016/j.compstruct.2014.03.012.

Irwin, P.A. (1984), "Wind tunnel tests of long span bridges. Poceedings of the 12th Congress IABSE, Vancouver, British Columbia, Canada.

Kubo, Y., *et al.* (2001), "Improvement of aeroelastic instability of shallow π section", *J. Wind Eng. Ind. Aerod.*, **89**(14), 445-1457. https://doi.org/10.1016/S0167-6105(01)00151-9.

Jorquera-Lucerga, J.J., Lozano-Galant J.A. and Turmo, J. (2016), "Structural behavior of non-symmetrical steel cable-stayed bridges", *Steel Compos. Struct.,* **20**(2), 447-468. https://doi.org/10.12989/scs.2016.20.2.447.

Ministry of communications of the People's Republic of China. (2004), "JTG/T D60-01-2004 Wind-resistant design specification for highway bridges", China Communications Press, Beijing, China.

Murakamia, T., Takedaa, K., Takaob, M. and Yuia, R. (2002), "Investigation on aerodynamic and structural countermeasures for cable-stayed bridge with 2-edge I-shaped girder", *J. Wind Eng. Ind. Aerod.*, **90**(6-7), 2143-2151.

Pedro, J.J.O. and Reis, A.J. (2010), "Nonlinear analysis of composite steel-concrete cable-stayed bridges", *Eng. Struct.*, **32**(9), 2702-2716. https://doi.org/10.1016/j.engstruct.2010.04.041.

Sakai, Y., *et al.* (1993), "An experimental study on aerodynamic improvements for edge girder bridges", *J. Wind Eng. Ind. Aerod.*, **49**(1-3), 459-466. https://doi.org/10.1016/0167-6105(93)90040-U.

Scanlan, R.H., and Tomko, J.J. (1971), "Airfoil and bridges deck flutter derivatives", *J. Eng. Mech.,* **97**(6), 1717-1733.

Scanlan, R.H. and Jones, N.P. (1990), "Aeroelastic analysis of cable-stayed bridges", *J. Struct. Eng.*, **116**(2), 279-297. https://doi.org/10.1061/(ASCE)0733-9445(1990)116:2(279).

Sears, W.R. (1941), "Aspects of non-stationary airfoil theory and its practical application", *J. Aerona Science.*, **8**, 104-108.

Selberg, A. (1963), "Aerodynamic effect on suspension bridges. In: Proc of int symposium on wind effects on buildings and structures", Teddington, England, 462-486.

Shehata, E. and Abdel, R. (2014), "Dynamic characteristics of hybrid tower of cable-stayed bridges", *Steel Compos. Struct.*, **17**(6), 803-8248. https://doi.org/10.12989/scs.2014.17.6.803.

Song, J.Z., Lin, Z.X. and Xu, J.Y. (2002), "Research and Appliance of Aerodynamic Measures about Wind-resistance of Bridges", *J. Tongji Uni (Natural Science Edition)*, **30**(5), 618-621. (In Chinese)

Van der Put. TACM (1976), "Rigidity of structures against aerodynamic forces", IABSE, 189-196.

Wang, X. and Wu, Z.S. (2010), "Evaluation of FRP and hybrid FRP cables for super long-span cable-stayed bridges", *Compos. Struct.*, **92**(10), 2582-2590. https://doi.org/10.1016/j.compstruct.2010.01.023.

Yang, Y.X. and Ge, Y.J. (2015), "Wind-resistant performance investigation for Shuitu Bridge. Technical Report WT201505", State Key Laboratory for Disaster Reduction in Civil Engineering, Shanghai. (In Chinese)

Yeh, F.Y., *et al.* (2015), "A novel composite bridge for emergency disaster relief: Concept and verification", *Compos. Struct.*, **127**(1), 199-210. https://doi.org/10.1016/j.compstruct.2015.03.012.

Zhang, W.M., Ge, Y.J. and Levitan, M.L. (2013), "Nonlinear aerostatic stability analysis of new suspension bridges with multiple main spans", *J. Braz. Soc. Mech. Sci. Eng.*, **35**(2), 143-151. https://doi.org/10.1007/s40430-013-0011-4.

Zhang, Y.Y., Song, X.G. and Zhang, Q.L. (2016), "Dynamic characteristics and wind-induced vibration coefficients of purlin-sheet roofs", *Steel Compos. Struct.*, **22**(5), 1039-1054. https://doi.org/10.12989/scs.2016.22.5.1039.

Zhou, R., *et al.* (2015), "Practical countermeasures for the aerodynamic performance of long span cable-stayed bridge with open deck", *Wind Struct.*, **21**(2), 223-229. https://doi.org/10.12989/was.2015.21.2.223.

Zhou, R., *et al.* (2018), "Comprehensive evaluation of aerodynamic performance of twin-box girder bridges with vertical stabilizers", *J. Wind Eng. Ind. Aerod.*, **175**, 317-327. https://doi.org/10.1016/j.jweia.2018.01.039.

Zhou, R., *et al.* (2019), "Nonlinear behaviors of the flutter occurrences for a twin-box girder bridge with passive countermeasures", *J. Sound Vib.*, **447**, 221-235. https://doi.org/10.1016/j.jsv.2019.02.002.

Zhu, L.D., Xiang, H.F. and Xu, Y.L. (2000), "Triple-girder model for modal analysis of cable-stayed bridges with warping effect", *Eng. Struct.*, **22**(10), 1313-1323. https://doi.org/10.1016/S0141-0296(99)00077-2.

BU